Open Access

Catalysis Research

LIDSEN Publishing Inc.

Research Article

Preparation and Characterization of Bimetallic Nanocatalyst Supported on Activated Carbon Prepared from Papaya Seeds

Abdul Rahman Y. Wahoud [1, *], Salim F. Bamsaoud [2], Mohammed F. Bamatraf [1], Qamar Al Zammar [3]

1. Department of Chemistry, College of Science, Hadhramout University, P.O.B. 50511, Mukalla, Yemen; E-Mails: awahoud8@gmail.com; g23120413003@hu.edu.ye
2. Department of Physics, College of Science, Hadhramout University, P.O.B. 50511, Mukalla, Yemen; E-Mail: saalem88@hu.edu.ye
3. Department of Chemistry, College of Science, Homs University, P.O.B. 77, Homs, Syria; E-Mail: qamaralza1997@gmail.com

* **Correspondence:** Abdul Rahman Y. Wahoud; E-Mail: awahoud8@gmail.com

Academic Editor: Pedro Fernandes

Catalysis Research
2026, volume 6, issue 2
doi:10.21926/cr.2602006

Received: January 15, 2026
Accepted: June 03, 2026
Published: June 16, 2026

Abstract

Preparation and characterization of an iron-tin bimetallic nanocatalyst supported on activated carbon (AC) prepared from papaya seeds, which was previously available in the surrounding environment, were performed. Different characterization techniques such as scanning electron microscopy (SEM), FT-IR spectrometry, and UV-Vis spectrophotometry were used. Many properties were characterized, and the resulting activated carbon could serve as an inexpensive catalytic support with a high surface area and a large micropore volume, even at a (20%) loading ratio of (Fe_2O_3-SnO_2/AC). Adsorption of methylene blue dye (MB) onto (Fe_2O_3-SnO_2/AC) surface was studied and optimal conditions were determined. The adsorption of methylene blue best fit the traditional Tempkin isotherm model, and the maximum capacity were 294.11 mg/g.

Keywords

Ferric oxide; tin dioxide; nanocatalyst; papaya seeds; activated carbon

1. Introduction

Many studies have investigated the use of activated carbon as a support for metal oxides, as an alternative to silica and alumina [1-6]. Nanoparticle catalysts supported on activated carbon are environmentally friendly and display enhanced activity due to the high surface area of the support [7-9]. Various agricultural wastes have been activated using different alkali hydroxides and carbonates, including coconut husk [10], cherry stone [11], date pits [12, 13], and papaya seeds [14]. Papaya seeds were selected because of their abundant availability and ease of activation [15, 16]. The optimal adsorption conditions were determined using the Taguchi design method [17, 18]. In our previous work, we prepared and characterized tin oxide supported on activated carbon derived chemically from date pits. In this work, we prepared and characterized a ferric oxide/tin oxide bimetal nanocatalyst supported on activated carbon chemically derived from papaya seeds. Papaya seeds contain a high percentage of fixed carbon and complex carbon structures such as lignin and cellulose, making them suitable as a low-cost, eco-friendly raw material for producing high-surface-area materials with outstanding adsorption capabilities and good physical and chemical properties. The optimal parameters for effective adsorption of methylene blue dye onto the prepared bimetal nanocatalyst were established using the Taguchi design method. This work demonstrates the potential applicability of the prepared material for the removal of pollutants from water and air, including industrial dyes, volatile organic compounds, heavy metals, and pharmaceuticals, thereby help migrate environmental pollution. The material may also serve as a catalyst in selected chemical reactions or as a carrier for catalytically active materials, such as metal nanoparticles or their oxides.

2. Materials and Methods

2.1 Chemicals

Ferrous chloride ($FeCl_2 \cdot 4H_2O$), stannous chloride ($SnCl_2 \cdot 2H_2O$), Sodium hydroxide (NaOH), Hydrochloric acid (HCl), iodine (I_2), starch, sodium thiosulfate ($Na_2S_2O_3$), glacial acetic acid (CH_3COOH), acetone, and methylene blue dye ($C_{16}H_{18}N_3SCl$, $3H_2O$) were used of analytical grade. A methylene blue stock solution (10 mmol/L) (Mw = 373.9 g/mol) was prepared and used in adsorption studies.

2.2 Treatment and Activation of Papaya Seeds

Papaya seeds were selected from agricultural waste from Mukalla/Hadhramaut/Yemen, where they are discarded in large quantities without effective use.

The collected papaya seeds were washed with water, dried at room temperature for 2 hours, then ground with a hand pestle and sieved to obtain a powder with a particle size of 0.5 mm, as shown in Figure 1. Then the powder was soaked in sodium hydroxide solution (30%) for 24 hours. The solution was then filtered, and the powder was placed in a furnace and heated to 450°C for two hours. The sample was then washed with 0.01 N hydrochloric acid until the filtrate became neutral. After that, the sample was dried at 110°C for 2 hours. In the present study, sodium

hydroxide (NaOH) was used in the preparation of activated carbons because it is cost-effective and easy to remove after activation with good performance [19]. The surface area was estimated mathematically from iodine number and methylene blue number [20]. Some of the prepared activated carbon and papaya seed properties are shown in Table 1.

Figure 1 Papaya seeds (left) and activated carbon (right).

Table 1 Properties of papaya seeds and activated carbon.

Properties	PS	AC
Ash%	1.8	0.4
Moisture%	5.8	2.3
Bulk density (g/ml)	0.65	0.34
Surface area (m^2/g)	397	691
Micropore volume (cm^3/g)	0.135	0.457
Total pore volume (cm^3/g)	0.476	0.738

2.3 Preparation of the Bimetallic Nanoparticals

The three chloride solutions ($SnCl_2$, $FeCl_2$, $SnCl_2$ + $FeCl_2$) were prepared using Acetic acid as the solvent [21]. Adding 2 g of $SnCl_2$ or $FeCl_2$ to 8 ml of deionized water and 4 ml of acetic acid and stirring for one hour. Then the solution was stirred for one hour at 90°C. This solution was put in the furnace for 1 hour at 400°C. For FeO_2-SnO_2 bimetallic, 1 g of $FeCl_2$ was mixed with 1 g of $SnCl_2$ powder and added to 8 ml, followed by the same previous preparation method [12].

2.4 Bimetallic Nanocatalyst Preparation

Bimetallic Fe_2O_3-SnO_2 nanoparticles were prepared by thermal decomposition using metal chlorides [21]. Each of the three obtained transparent solutions was loaded onto prepared activated carbon from papaya seeds, at a 20% metal/activated carbon, and stirred for 1 hour at 110°C until dried. Finally, it was placed in an oven for 2 hours at 400°C to obtain oxide nanoparticles. The reactions can be described as below [22]:

$$FeCl_2 + SnCl_2 \xrightarrow{\text{Aqueous solution}} Fe^{2+} + Sn^{2+} + 4Cl^-$$

$$Fe^{2+}+Sn^{2+}+CH_3COOH \xrightarrow{\text{Aqueous solution}} (CH_3COO)_2Sn\text{-}Fe+2H^+$$

$$(CH_3COO)_2Sn\text{-}Fe \xrightarrow{\text{Oxidation 400°C}} Fe_2O_3+SnO_2+CO_2+CO$$

$$Fe_2O_3+SnO_2+AC \xrightarrow{\text{Aqueous solution}} [(CH_3COO)_2Sn\text{-}Fe(AC)]$$

$$[(CH_3COO)_2Sn\text{-}Fe(AC)] \xrightarrow{\text{Heat Treatment}} Fe_2O_3\text{-}SnO_2(AC)+CO_2$$

2.5 Taguchi Statistical Method

The L_9 array was used to determine the best parameters for maximum adsorption. A set of three-factor experiments with three levels is shown in Table 2. The signal-to-noise (S/N) ratio was calculated from the equation below [17, 18]. The larger the value of (S/N), the better.

$$\frac{S}{N} = 10\log\frac{(1/Y_1^2 + 1/Y_2^2 + \cdots + 1/Y_n^2)}{n} \quad (1)$$

Table 2 Levels and factors.

Factor	Level 1	Level 2	Level 3
Contact time (min)	15	30	60
Initial conc. (mmol/L)	1	2.5	5
Temperature (K)	293	313	333

2.6 Adsorption Isotherm

Adsorption isotherms were determined by stirring 50 mL of dye solutions at different concentrations with 0.5 g of adsorbent at ambient temperature until equilibrium was reached. Then the samples were measured by a UV-Vis Spectrometer at λ = 665 nm. The uptake qt was calculated from the equation below:

$$q_t = \frac{(C_0 - C_t)}{W} \times V \quad (2)$$

Where: C_0 and C_t are the concentrations before and after dye adsorption, respectively; V (L) is the volume; and W (g) is the weight of the adsorbent.

2.7 Ash and Moisture Content Determination

To determine the ash content, 0.5 g of the adsorbent was weighed in a pre-weighted ceramic crucible. After that, the sample was heated to 750°C for 3 hours. Ash percent was calculated as below:

$$\text{Ash}\% = \frac{W_3 - W_2}{W_1} \times 100 \quad (3)$$

To determine moisture content, 0.25 gram of adsorbent was placed into the crucible in the oven at 110°C. Then the sample was allowed to cool. The moisture content was calculated as below:

$$\text{Moisture}\% = \frac{W_4 - W_2}{W_1} \times 100 \quad (4)$$

W_1 is the original adsorbent weight (g), W_2 the crucible weight (g), W_3 the crucible with ash weight (g), W_4 the crucible with dried adsorbent weight (g).

2.8 Iodine Number (IN) Determination

Iodine number (IN) (mg/g) measures the level of carbon activation. A higher iodine number means higher degree of activation and higher micropore content. To determine the iodine number, 0.05 g of the adsorbent was titrated with sodium thiosulfate. The iodine number was calculated by the equation below:

$$IN\ (\text{mg/g}) = \frac{(V_b - V_s) \cdot N \cdot (126.9) \cdot 15/10}{M} \quad (5)$$

V_b (ml) and V_s (ml) are volumes of sodium thiosulfate for blank and sample (ml), respectively, M (g). is the mass of adsorbent.

2.9 Instruments

Chemical functional groups were identified by an FT-IR spectrophotometer 4600- Jasco/Japan using KBr pellets, where a small amount of adsorbent was mixed with milligrams of KBr and manually pressed under 8 tons. The frequency range was measured between (400-4000 cm^{-1}). Muffle Furnace model (FB1310M) from Thermolyne/U.S.A with a thermostat to control and program temperature up to 1300°C (1573 K) was used to prepare the adsorbents, dry the samples, and measure the moisture and ash content. To study the morphology of papaya seeds, prepared activated carbon and Fe_2O_3-SnO_2/AC surfaces, scanning electron microscopy (SEM) from the FEI company model Quanta 200 was used.

3. Results and Discussion

3.1 Infrared Spectroscopy Characterizations

Figure 2 shows FT-IR spectra of papaya seeds and the prepared activated carbon, illustrating the chemical functional groups. O–H stretching vibration band at 3400 cm^{-1} is from hydroxyl groups, phenols, or alcohols, and the position of this band at a lower wavenumber may be due to adsorbed water from the surroundings. In contrast, the C–H aliphatic stretching vibration bands appear at 2924 cm^{-1} and at 2854 cm^{-1} [23]. The peak in the region of ≈1650 cm^{-1} has been observed by C=C stretching absorption while C-O stretching peak at 1100 cm^{-1} may be belong to phenols and esters groups at the surface of adsorbent [24, 25]. The presence of hydroxyl groups, carbonyl groups, and aromatic compounds in adsorbents, which play important roles in the adsorption process, provides evidence of the lignocellulosic structure of papaya seeds. Two bands

at 1745 and 1634 have changed into a strong sharp peak at 1556 cm^{-1} ascribed to C=O conjugated with C=C stretching vibration, like a highly conjugated C=O stretching in carboxylic groups. This indicates an increase in oxygen content on the surface after activation. This result was observed in other materials such as Tunisian olive-waste cakes [26] and lignocellulose.

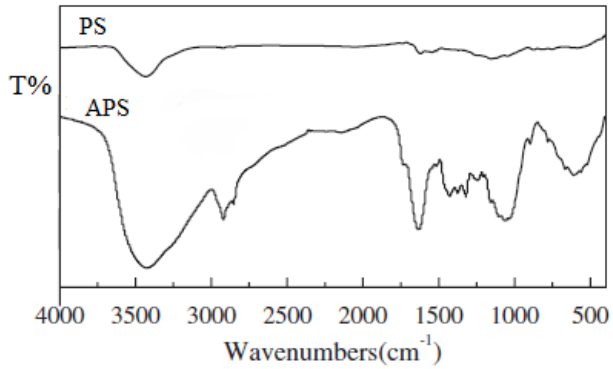

Figure 2 FT-IR of papaya seeds (ps), activated carbon (Aps).

3.2 Ultraviolet Spectrum of Solutions Depicted

UV-Vis absorption spectrum for the transparent Fe_2O_3-SnO_2, Fe_2O_3 and SnO_2 solutions (Figure 3) shows a absorption narrow peak between 278-295 nm. UV-Vis absorption spectrum of SnO_2 nm has an absorption peak at 295nm, which corresponds to a band gap of 4.1 eV, indicating a nanoparticle size corresponding to a bulk Bohr exciton radius equal to 2.8 nm. The Fe_2O_3 UV-Vis absorption has narrow band at 280 nm, the absorption spectra Fe_2O_3/SnO_2 showed a blue shift and the peak was found to be at 278 nm calculated optical band gap of ~4.48 eV [27].

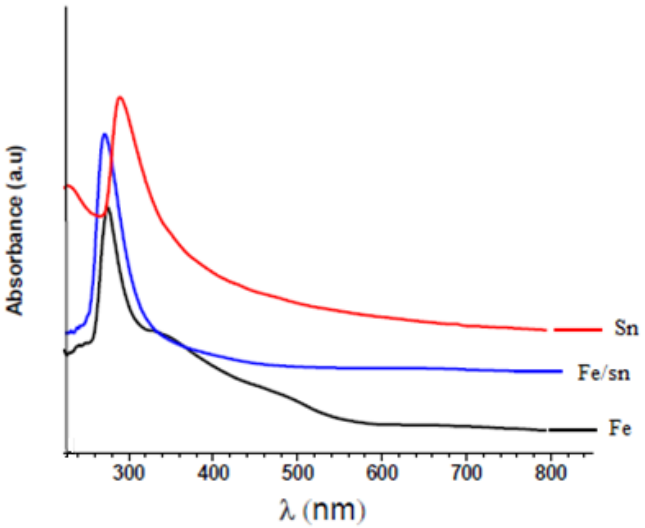

Figure 3 UV-Vis spectra of the transparent Fe_2O_3-SnO_2, Fe_2O_3 and SnO_2 solutions.

3.3 The Scanning Electron Microscope (SEM)

The SEM images of the papaya seed surface, shown in Figure 4, indicate that the papaya powder particles are spherical, with a particle size of about 3 µm, while the prepared activated carbon is cracked and scattered, with a smaller particle size compared to papaya powder particles.

In agreement with the data from the ultraviolet spectrum. The SEM images for SnO_2 and Fe_2O_3 Figure 5 show that the nanoparticle size was about 80 nm. The SEM image of the Fe_2O_3-SnO_2/AC surface Figure 6 indicates the nanostructures of Fe_2O_3-SnO_2/AC, which shows a good dispersion of Fe_2O_3 and SnO_2 on the surface of activated carbon [13].

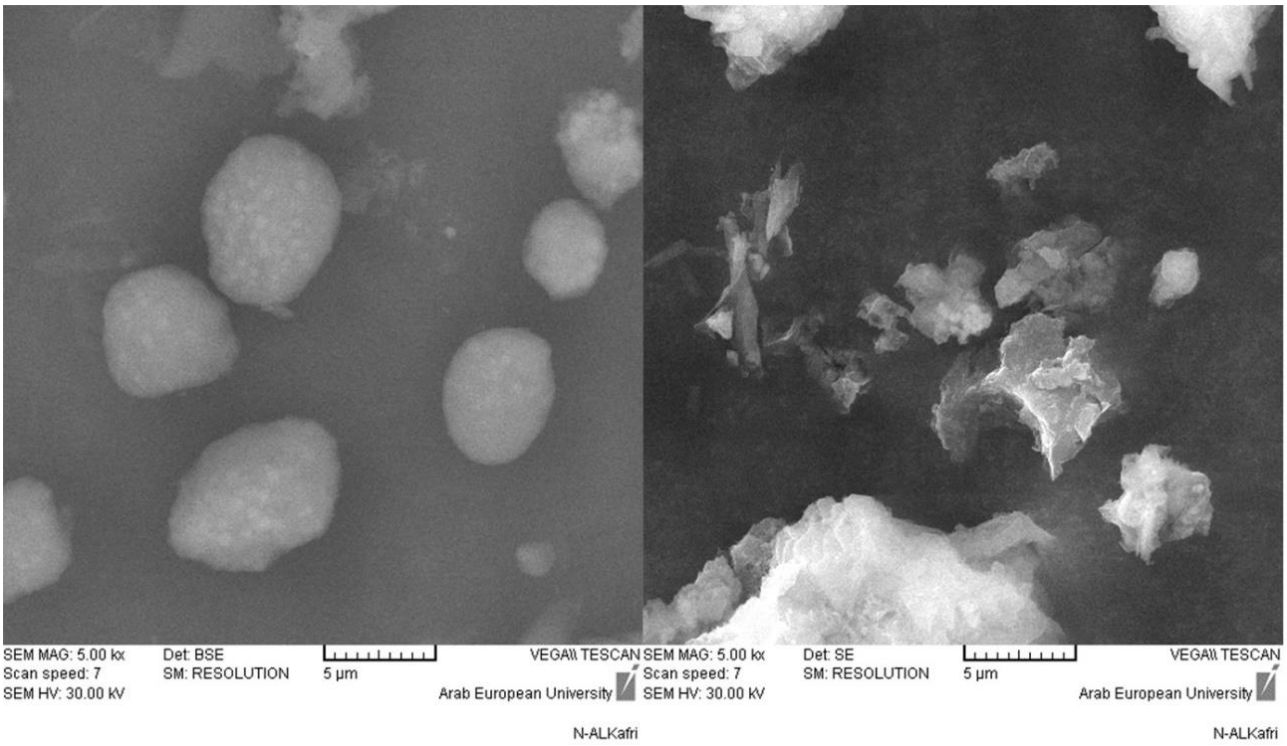

Figure 4 SEM papaya seeds (left), activated carbon (right).

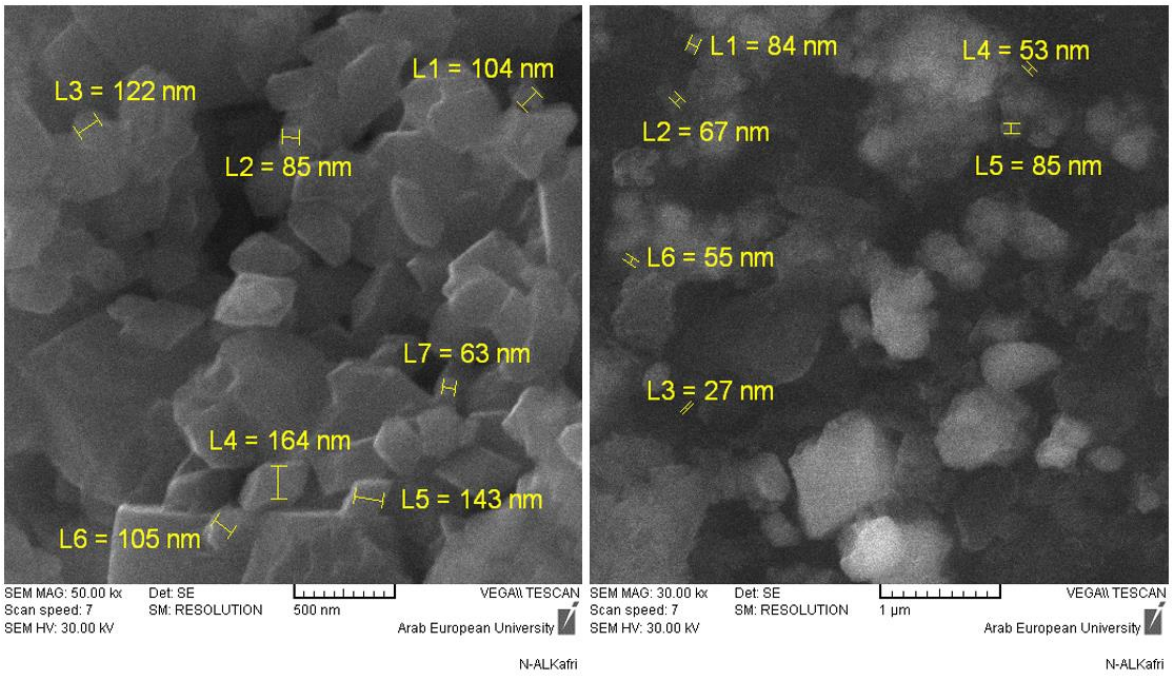

Figure 5 SEM of SnO_2 (left), Fe_2O_3 (right).

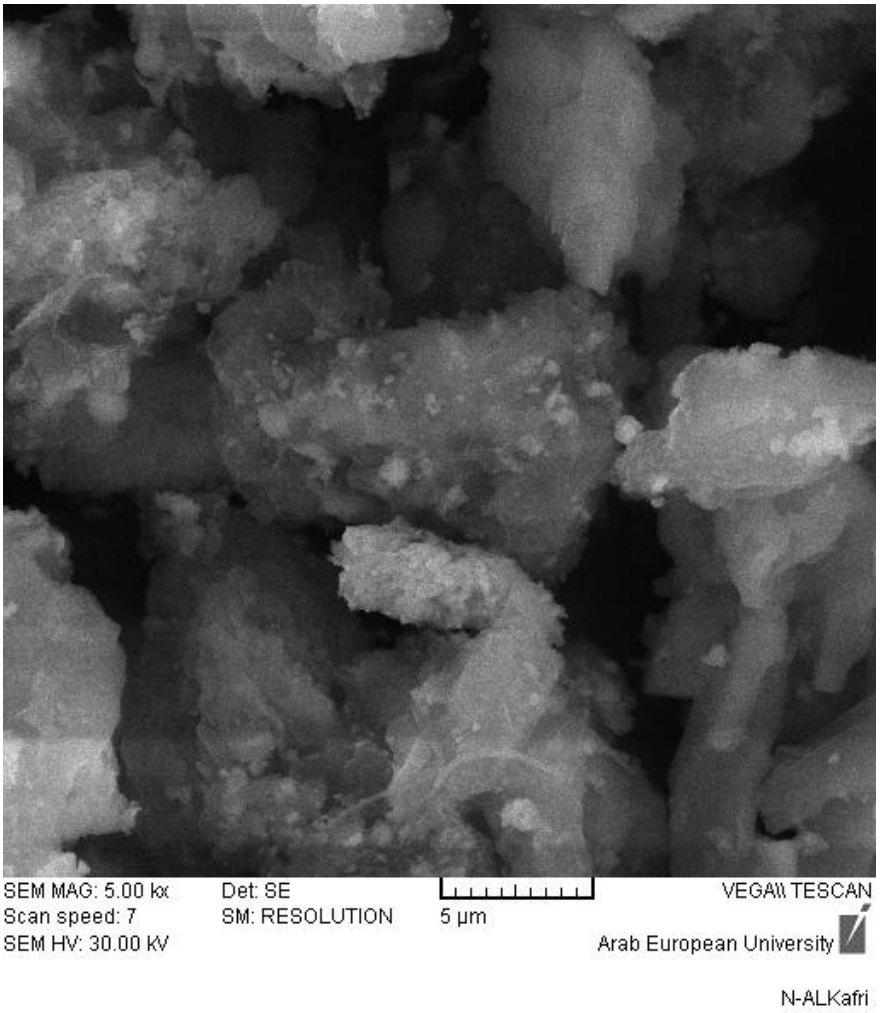

Figure 6 SEM of Fe_2O_3-SnO_2/AC surface.

3.4 Iodine Number, Surface Area and Pore Structure

There are three types of pore size: micropore (less than 2 nm), mesopore (2-50 nm), and macropore (more than 50 nm). The porous volume and the surface area were calculated from iodine number and methylene blue number [20]. The results were put in Table 3, which shows that the surface areas and pore volumes were increased by chemical activation of the papaya seeds because chemical activation led to the development of micropores in the prepared activated carbon, increasing the porosity and surface area. The nanocatalyst 20% Fe_2O_3-SnO_2/AC has less porosity than the activated carbon because the metals close the pores. However, they haven't affected it so much, and the Fe_2O_3-SnO_2/AC 20% nanocatalyst still has a high surface area of 594 cm^2/g with a large micropore volume of 0.291 cm^3/g and a large total pore volume of 0.616 cm^3/g, this indicates that the nanoparticles don't agglomerate and don't block the pores. They don't crystallize outside of the pores.

Table 3 Surface area and porosity of Fe_2O_3-SnO_2/AC.

	APS	Fe_2O_3-SnO_2/AC
Iodine number (mg/g)	690	610
Methylene blue number (mg/g)	280	220
Surface area (m^2/g)	691	594
Micropore volume (cm^3/g)	0.457	0.291
Total pore volume (cm^3/g)	0.738	0.616

3.5 Adsorption Studies

3.5.1 Effect of Contact Time and Initial Concentration

To study the effect of contact time and initial concentration, the uptakes were plotted in Figure 7 versus contact time with different initial concentrations (1, 2.5, and 5 mmol/L) for the dye with a ratio of 0.25 g of adsorbent to 50 mL of the dye solution. The mixture of different concentrations were shaken for different time intervals (15, 30, 60, 90 and 120 min.) at 293 K. It is clearly that the uptake of adsorbents first increase rapidly with increasing of contact time to reach equilibrium time and remained constant after that due to the fast adsorption at the initial stage may be due to the higher driving force making fast transfer of dyes ions to the surface of nanoparticles and the availability of the uncovered surface area and active sites on the adsorbent. Maximum uptake was 313.17 mg/g, 157.21 mg/g and 63.31 mg/g with 5 mmol/L, 2.5 mmol/L and 1 mmol/L initial concentration of MB respectively, so it's clear the adsorption capacity dependent on initial dye concentration which provides necessary driving force making fast transfer of dye ions to the surface of FeO_2-SnO_2/AC to overcome all resistance to mass transfer of dyes between the aqueous and solid phase [28].

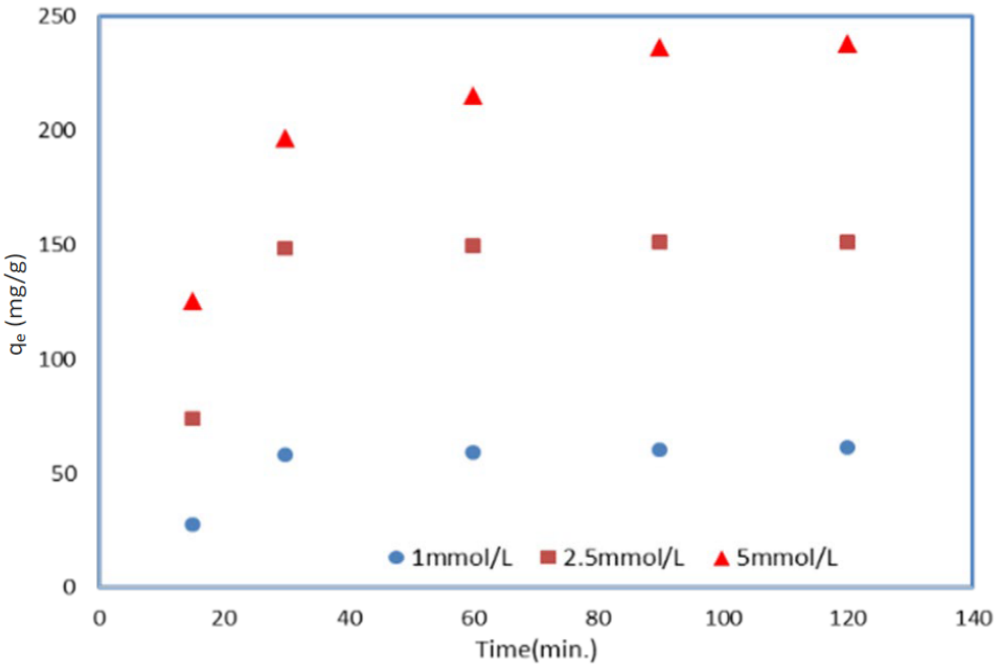

Figure 7 Effect of contact time and initial MB concentration on adsorption at 293 K.

3.5.2 Taguchi Statistical Method

The L_9 array was designed to study the Effects of different parameters on MB dye adsorption onto the FeO_2-SnO_2/AC nanocatalyst. The results of experiments in Table 4 show that the uptake of MB varied from 32.49 mg/g to 237.96 mg/g and S/N ratios from 30.23 to 47.53. From Table 5 and Figure 8, it is clear that the ideal parameters for adsorption are contact time 60 min, initial MB concentration 5 mmol, and temperature 298 K. It can be observed that the initial dye concentration factor is the most significant controllable factor of MB adsorption into the Fe_2O_3-SnO_2/AC nanocatalyst. On the other hand, the uptake amount obtained by the Taguchi method is 237.96 mg/g, which is very close to the experimental uptake amount under the same conditions, with 267.45 mg/g. The thermodynamic behavior of the MB adsorption shows that the uptake decreases with increasing temperature, which indicates an exothermic nature. This may be due to the weak attraction between MB and the adsorbent surface. Figure 9 shows that the MB molecules escape from the surface into the bulk phase [19].

Table 4 L_9 Statistical arrays.

Contact time (min)	Initial conc. (mmol/L)	Temp. (K)	Uptake mg/g	S/N ratio
15	1	293	40.23	32.09
15	2.5	313	70.77	36.99
15	5	333	92.54	39.32
30	1	333	53.22	34.52
30	2.5	313	137.77	42.78
30	5	293	205.11	46.23
60	1	313	58.65	35.36
60	2.5	333	151.88	43.63
60	5	293	237.96	47.53

Table 5 Response of S/N and factor contributions.

Level	Contact time (min)	Initial conc. (mmol/L)	Temperature (K)
1	35.89	33.79	40.06
2	41.28	41.17	39.33
3	42.14	44.34	39.47
Delta	7.25	10.55	0.59
Rank	2	1	3

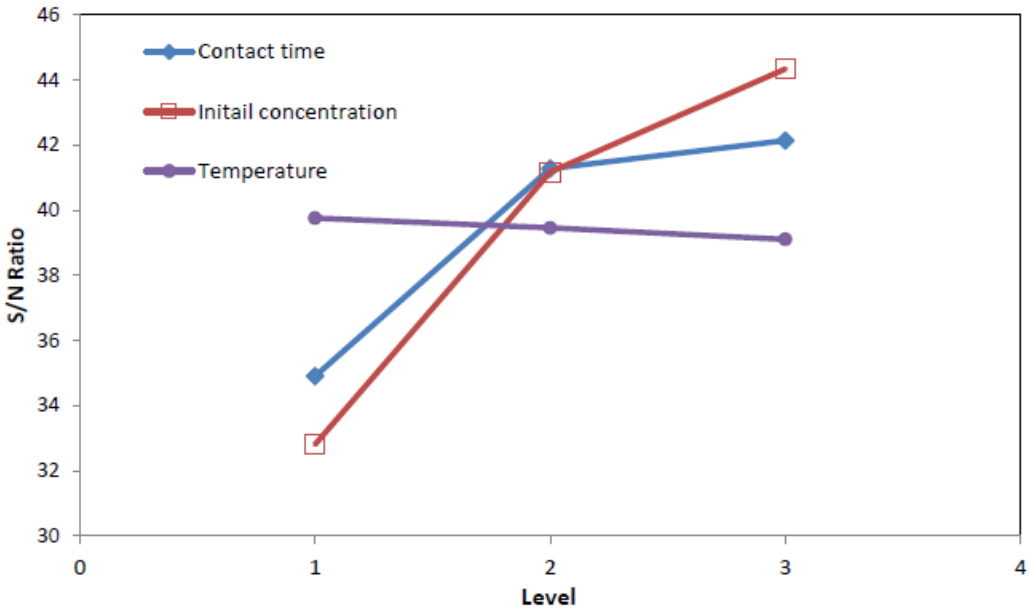

Figure 8 The plot of S/N ratios versus factor levels of parameters for MB adsorption onto FeO_2-SnO_2/AC.

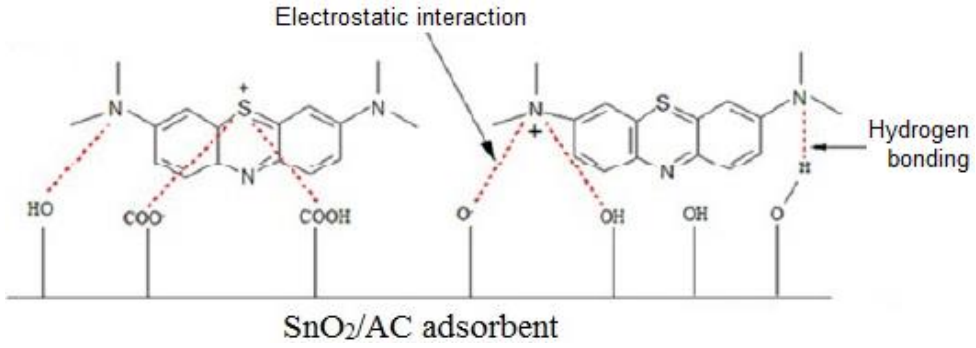

Figure 9 Mechanism of MB adsorption on FeO_2-nO_2/AC.

3.5.3 Adsorption Isotherms

Three models, Langmuir Eq. (6), Freundlich Eq. (7), and traditional Tempkin Eq. (8) of adsorption isotherms, were applied. The experimental data for the MB dye adsorption and the calculated constants from the three isotherm equations (6), (7), (8) were put in Table 6. The higher R^2 value of the adsorption isotherm, the more accurately the isotherm model describes the adsorption behavior [29]. Therefore, the Tempkin model provided a better fit than the Langmuir and Freundlich models. Moreover, in agreement with the amount obtained by the Taguchi method, the adsorptive capacity (q_m) of MB onto Fe_2O_3-SnO_2/AC was 294.118 mg/g.

$$\frac{1}{q_e} = \frac{1}{K_L q_m}\frac{1}{C_e} - \frac{1}{q_m} \tag{6}$$

$$\log q_e = \log K_f + \frac{1}{n}\log C_e \tag{7}$$

$$q_e = B_T \ln K_T + B_T \ln C_e \tag{8}$$

Where: C_e (mg/L) is the equilibrium dye concentration, K_L is Langmuir constant, K_f and n are Freundlich constants, B_T (J/mol) is Tempkin constant related to the heat of adsorption, and K_T (L/mg) is Empirical Tempkin constant related to the maximum binding energy.

Table 6 Isotherm model parameters for adsorption.

Langmuir Parameters	Q_m (mg/g)	294.118
	K_L (L/mg)	0.021
	R_L	0.029
	R^2	0.9943
Freundlich Parameters	K_f (mg/g)	28.347
	1/n	0.3698
	R^2	0.8795
Tempkin Parameters	K_T (L/mg)	0.332
	B_T (J/mol)	49.702
	R^2	0.99694

4. Conclusion

FeO_2-SnO_2 nanoparticle powders were successfully synthesized through a simple precipitation method at 70°C by dissolving $FeCl_2$ and $SnCl_2$ in water, followed by the addition of glacial acetic acid. The results clearly demonstrate that activated carbon is a suitable, inexpensive support for preparing Fe_2O_3-SnO_2 as a high-surface-area nanocatalyst, even at a high 20% ratio, and could pave the way toward environmentally friendly reactions. Among the three studied adsorption isotherms, the traditional Tempkin isotherm was found to be the best model for MB dye adsorption onto the prepared Fe_2O_3-SnO_2/AC, with a maximum capacity equal to 294.11 mg/g. Functional groups in the produced activated carbon were identified by the infrared spectrum, such as OH, CH, and CO, and aromatic compounds, which play an important role in the adsorption process. The oxygen content increased after chemical activation with sodium hydroxide.

Author Contributions

Dr. Abdul Rahman Y. Wahoud and Dr. Salim F. Bamsaoud suggest the main ideas and experimental of this research and write the all manuscript and design the figure in Excel Microsoft, Mr. Mohammed F. Bamatraf have done the all experiments and lab works while Mrs. Qamar Al Zammar contribute with the SEM photos and helping in lab works.

Competing Interests

The authors declare that no competing interests exist.

References

1. Wahoud A, Alouche A, Abdulbake M. Sulfuric acid baking and leaching of spent sulfuric acid catalyst. Period Polytech Chem Eng. 2011; 55: 31-34.

2. Wahoud A, Khorfan S, Reda Y. Recovery of vanadium pentoxide from spent catalyst used in the manufacture of Sulphuric acid. Period Polytech Chem Eng. 2001; 45: 131-137.
3. Huang JS, Huang ZC, Liu TY, Chen JS, Wang JQ, Rokhum SL, et al. One-step photothermal synthesis of biofuels from high-acid-value non-edible oils with adjacent Cs single atoms at ambient conditions. Rare Metals. 2025; 44: 5529-5543.
4. Huang J, Jian Y, Li H, Fang Z. Lignin-derived layered 3D biochar with controllable acidity for enhanced catalytic upgrading of Jatropha oil to biodiesel. Catal Today. 2022; 404: 35-48.
5. Huang J, Liu T, Wang K, Huang Z, Wang J, Rokhum SL, et al. Room-temperature and carbon-negative production of biodiesel via synergy of geminal-atom and photothermal catalysis. Environ Chem Lett. 2024; 22: 1607-1613.
6. Chimentão RJ, Herrera JE, Kwak JH, Medina F, Wang Y, Peden CH. Oxidation of ethanol to acetaldehyde over Na-promoted vanadium oxide catalysts. Appl Catal A Gen. 2007; 332: 263-272.
7. Tanaka A, Yoon SH, Mochida I. Formation of fine Fe–Ni particles for the non-supported catalytic synthesis of uniform carbon nanofibers. Carbon. 2004; 42: 1291-1298.
8. Huwe H, Fröba M. Synthesis and characterization of transition metal and metal oxide nanoparticles inside mesoporous carbon CMK-3. Carbon. 2007; 45: 304-314.
9. Huwe H, Fröba M. Iron(III) oxide nanoparticles within the pore system of mesoporous carbon CMK-1: Intra-pore synthesis and characterization. Microporous Mesoporous Mater. 2003; 60: 151-158.
10. Tan IA, Ahmad AL, Hameed BH. Adsorption of basic dye on high-surface-area activated carbon prepared from coconut husk: Equilibrium, kinetic and thermodynamic studies. J Hazard Mater. 2008; 154: 337-346.
11. Lussier MG, Shull JC, Miller DJ. Activated carbon from cherry stones. Carbon. 1994; 32: 1493-1498.
12. Wahoud AY, Bamsaoud SF, Almagdi S, Al-Haiqi MA. Effective adsorption of basic dye onto different carbon kinds prepared from date stones based on Taguchi design method, kinetic and thermodynamic. J Phys Conf Ser. 2021; 1900: 012003.
13. Wahoud AR, Bamsaoud SF, Al-Haiqi MA. Preparation and characterization of SnO_2/AC as a novel high surface area nanocatalyst. Period Polytech Chem Eng. 2021; 65: 343-349.
14. Krishni RR, Foo KY, Hameed BH. Adsorption of methylene blue onto papaya leaves: Comparison of linear and nonlinear isotherm analysis. Desalin Water Treat. 2014; 52: 6712-6719.
15. Belala Z, Jeguirim M, Belhachemi M, Addoun F, Trouvé G. Biosorption of basic dye from aqueous solutions by Date Stones and Palm-Trees Waste: Kinetic, equilibrium and thermodynamic studies. Desalination. 2011; 271: 80-87.
16. Hameed BH, Salman JM, Ahmad AL. Adsorption isotherm and kinetic modeling of 2,4-D pesticide on activated carbon derived from date stones. J Hazard Mater. 2009; 163: 121-126.
17. Rahmani M, Kaykhaii M, Sasani M. Application of Taguchi L16 design method for comparative study of ability of 3A zeolite in removal of Rhodamine B and Malachite green from environmental water samples. Spectrochim Acta A. 2018; 188: 164-169.
18. Ghasemi M, Mashhadi S, Azimi-Amin J. Fe_3O_4/AC nanocomposite as a novel nano adsorbent for effective removal of cationic dye: Process optimization based on Taguchi design method, kinetics, equilibrium and thermodynamics. J Water Environ Nanotechnol. 2018; 3: 321-336.

19. Manna S, Roy D, Saha P, Gopakumar D, Thomas S. Rapid methylene blue adsorption using modified lignocellulosic materials. Process Saf Environ Prot. 2017; 107: 346-356.
20. Nunes CA, Guerreiro MC. Estimation of surface area and pore volume of activated carbons by methylene blue and iodine numbers. Quím Nova. 2011; 34: 472-476.
21. Sharma G, Kumar A, Sharma S, Naushad M, Dwivedi RP, ALOthman ZA, et al. Novel development of nanoparticles to bimetallic nanoparticles and their composites: A review. J King Saud Univ Sci. 2019; 31: 257-269.
22. Okhiopkova L, Khitsova M, Ismagilov Z. Prepration of bimetallic oxide on carbon supports: The effect of the support on the stability of catalysts to thermal decomposition. Chem Sustain Dev. 2021; 29: 582-588.
23. Acevedo B, Barriocanal C, Lupul I, Gryglewicz G. Properties and performance of mesoporous activated carbons from scrap tyres, bituminous wastes and coal. Fuel. 2015; 151: 83-90.
24. Abdus-Salam N, Ikudayisi-Ugbe AV, Ugbe FA. Adsorption studies of acid dye–Eosin yellow on date palm seeds, goethite and their composite. Chem Data Collect. 2021; 31: 100626.
25. Asbollah MA, Mahadi AH, Kusrini E, Usman A. Synergistic effect in concurrent removal of toxic methylene blue and acid red-1 dyes from aqueous solution by durian rind: Kinetics, isotherm, thermodynamics, and mechanism. Int J Phytorem. 2021; 23: 1432-1443.
26. Mameri N, Aioueche F, Belhocine D, Grib H, Lounici H, Piron DL, et al. Preparation of activated carbon from olive mill solid residue. J ChemTechnol Biotechnol. 2000; 75: 625-631.
27. Zhou W, Liu Y, Yang Y, Wu P. Band gap engineering of SnO_2 by epitaxial strain: Experimental and theoretical investigations. J Phys Chem C. 2014; 118: 6448-6453.
28. Ramamoorthy M, Ragupathy S, Sakthi D, Arun V, Kannadasan N. Synthesis of SnO_2 loaded on corn cob activated carbon for enhancing the photodegradation of methylene blue under sunlight irradiation. J Environ Chem Eng. 2020; 8: 104331.
29. Haghbin MR, Shahrak MN, LotfiKatooli L, Mirzaei S. Potential of green-based microporous carbon for advanced water decontamination from azo dyes: Experiment and molecular dynamic simulation studies. J Environ Chem Eng. 2024; 12: 111875.